PIER M

(Received 13 October 2023, Accepted 23 February 2024, Scheduled 5 March 2024)

A Compact, High Gain Ring Metamaterial Unit Cell Loaded Triple Band Antenna for 5G Application

KM Neeshu[1] and Anjini Kumar Tiwary[2,*]

[1] *Electronics & Communication (ECE), Birla Institute of Technology Mesra, Ranchi, Jharkhand, India*
[2] *Electronics & Communication, Birla Institute of Technology, Mesra, Ranchi, Jharkhand, India*

ABSTRACT: A novel planer, compact and quarter-wave transformer-coupled fed multi-band antenna is proposed and designed. The antenna uses a split-ring resonator (SRR) inspired ring metamaterial unit cell. The proposed ring metamaterial unit cell gives single negative (Epsilon negative) behaviour, which improves antenna performance. A partial ground and a quarter-wave transformer-coupled feed line are used to improve the impedance matching of the antenna. The antenna gives multi-band operation at resonating frequencies, 3.5, 8.5, and 13.7 GHz, with 2.9–4.5 GHz, 8.0–10.34 GHz, and 12.3–14.3 GHz, respectively. The maximum gains at resonating frequencies are 1.5 dBi, 4.1 dBi, and 6.5 dBi, with good impedance matching. The novelty of the antenna design is that the loading of the ring unit cell gives resonance at a much smaller wavelength than the resonant wavelength. The proposed antenna provides a miniaturized and multiband response compared to a conventional patch antenna.

1. INTRODUCTION

In a modern wireless communication system, an antenna that comprises multiple wireless standards for providing multiple applications such as Wi-Fi, Wi-MAX, and RFID is required. This antenna is known as a multi-band antenna, and it reduces the space and cost of the system. Microstrip antenna [1, 2] has low profile, light weight, easy integration, and low cost compared to conventional horn and Yagi-Uda antenna. These advantages of the microstrip antenna make it more suitable and flexible for multi-band antenna design. One of the basic techniques to implement a multi-band antenna is integrating multiple resonating elements, modifying radiating patch and ground plane in a microstrip patch antenna. In [3, 4], a dipole with two different arm lengths, using a shorting pin between ground and patch [5, 6], and parasitic elements in laptop application [7] result in two resonating frequency bands. Triple and quad-band [8, 9] patch antennae are discussed using trapezoidal and crinkle fractal shapes. However, these conventional designs compromise antenna and structure simplicity, which results in low efficiency and importable antenna.

Metamaterials are artificial materials that exhibit unnatural properties [10, 11], such as negative permittivity, permeability, and reversal of Snell law. These properties are derived from their sub-wavelength configurations rather than material, resulting in left-hand wave propagation [12]. Metamaterial is used to design a multi-band antenna [13, 14] with the loading of SRR and complementary SRR (CSRR) in rectangular patch antenna and hexagon patch antenna, respectively. Eleftheriades and Antoniades presented a dipole antenna with the metamaterial transmission line [15] for multiband response. The design validation approach is reported in [16, 17] to achieve a multi-band antenna. The multi-band and miniaturization of antenna [18, 19] using metamaterial unit cell loading is proposed. In some work, offset feed is used to achieve impedance matching, resulting in poor antenna co-cross. However, the radiation pattern cannot be kept symmetric in the E-plane and omnidirectional in the H-plane due to the asymmetric design. This work discusses the design and characterization of multi-bands loaded with a metamaterial unit cell fed by a quarter-wave transformer-coupled feed line. The metamaterial unit cell consists of four quad rings under a circular ring to create additional resonance. Moreover, a quarter-wave transformer-coupled feed line is used to achieve a better cross-polarization. In the end, partial ground planes are employed which improves the antenna's impedance matching. The proposed antenna is designed and optimized by the CST microwave studio simulation software based on the finite integration (FIT) method.

2. UNIT CELL DESIGN

The metamaterial ring unit cell is shown in Figure 1. The unit cell dimension is comparable to $\lambda_g/8$, which confirms the metamaterial periodic condition that the size of the metamaterial unit cell should be less than $\lambda_g/4$. Figure 1(a) shows the front view of the ring unit cell, which is connected by four quad circles. Here, the shape of the unit cell is chosen as circle because it eliminates the sharp edge discontinuities of electromagnetic (EM) waves. Four quad circles utilize the inner space more efficiently than the conventional split-ring resonator. The intra-coupling between the outer ring and four quad circles results in lower frequency shifts. Thus, the unit cell's loading helps achieve a miniaturized response compared to a conventional patch antenna. Figure 1(b) depicts the unit cell's back view. The sizes of the top and bottom unit cells are the same.

* Corresponding author: Anjini Kumar Tiwary (aktiwary@bitmesra.ac.in).

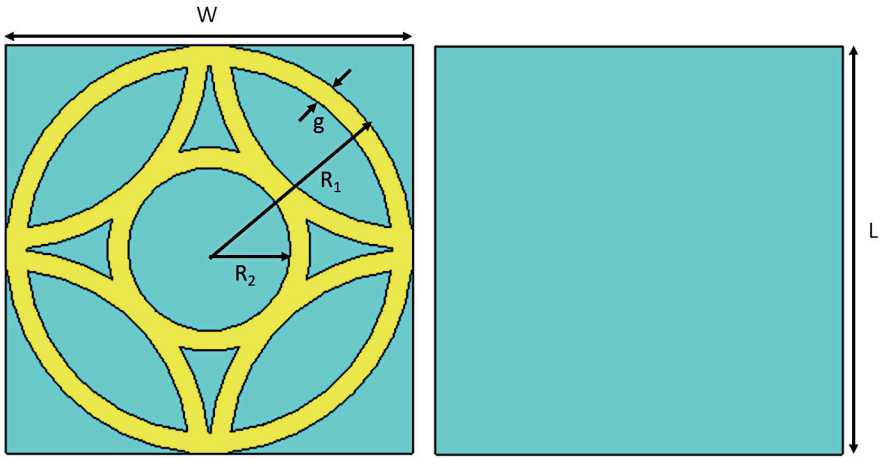

FIGURE 1. Geometry of the proposed unit cell: (a) Front view, (b) back view.

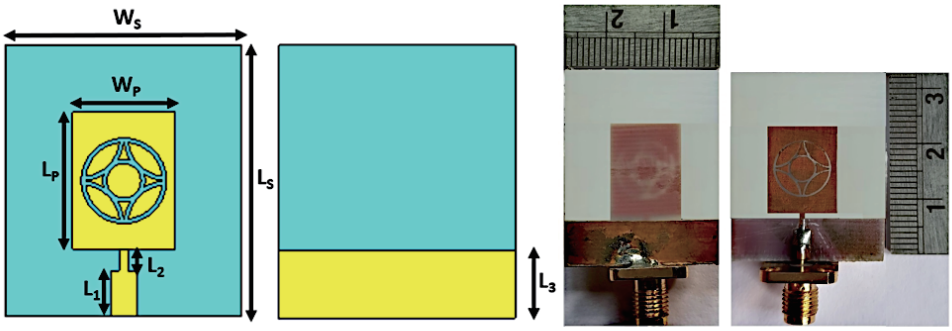

FIGURE 2. Schematic presentation of the compact planer dual-band antenna. (a) Front view. (b) Back view.

The dimensions of the proposed unit cell, as shown in Figure 1, are $W = L = 10\,\text{mm}$, $R_1 = 5\,\text{mm}$, $R_2 = 2.5\,\text{mm}$, $g = 0.5\,\text{mm}$.

3. ANTENNA DESIGN AND ITS EQUIVALENT CIRCUIT MODEL

Figures 2(a) & (b) show the proposed metamaterial-loaded multi-band antenna design. The antenna is fabricated on an FR-4 epoxy substrate of relative permittivity 4.4, loss tangent 0.025, and thickness 1.6mm. The fabricated prototype of the antenna is shown in Figures 2(c) & (d). Figure 2(a) depicts that the metamaterial ring unit cell is loaded in the conventional patch, which gives a lower shift in frequency; thus, a miniaturized response of the antenna is achieved. It is difficult to accomplish impedance matching of the electrically small antenna due to low radiation resistance and high reactance. To overcome this, the patch antenna is fed by a quarter transformer-coupled feed line at the center of the patch, which helps eliminate asymmetric radiation patterns and improve the co-cross polarization of the antenna. The impedance matching can be improved if the input impedance of the antenna (Z_a) matches the impedance of the feed line (Z_o). The input impedance at the beginning of the quarter-wavelength Z_q can be calculated by putting

$$Z_{in} = Z_o, Z_{in} = Z_o = \left(Z_q^2\right)/Z_a$$

$$Z_q = \sqrt{(50 * Z_a)}$$
$$\text{where} \quad Z_a = \left(90\epsilon_r^2\right)/(\epsilon_r - 1)(L/W)^2$$

The antenna is loaded with a negative permittivity unit cell. Due to this loading of high permittivity, the metamaterial unit cell antenna suffers from narrow bandwidth. This can be overcome by reducing the ground plane length. Also, the ground at the back of the antenna interprets impedance matching of the antenna; thus, a partial ground is used. Reducing ground plane length to a certain value affects the electromagnetic coupling between the radiating patch and the ground plane, resulting in better impedance matching and bandwidth improvement. The antenna is expected to give two resonant modes. The higher resonance is due to the conventional patch antenna, and the lower mode is excited because of the coupling effect due to the loading of the metamaterial unit cell. The effects of each design step are discussed in the result section. The optimized dimensions of the proposed antenna are $W_s = 27.6\,\text{mm}$, $L_s = 31.8\,\text{mm}$, $W_p = 12\,\text{mm}$, $L_p = 16\,\text{mm}$, $L_1 = 5.3\,\text{mm}$, $L_2 = 2.6\,\text{mm}$, and $L_3 = 7.9\,\text{mm}$.

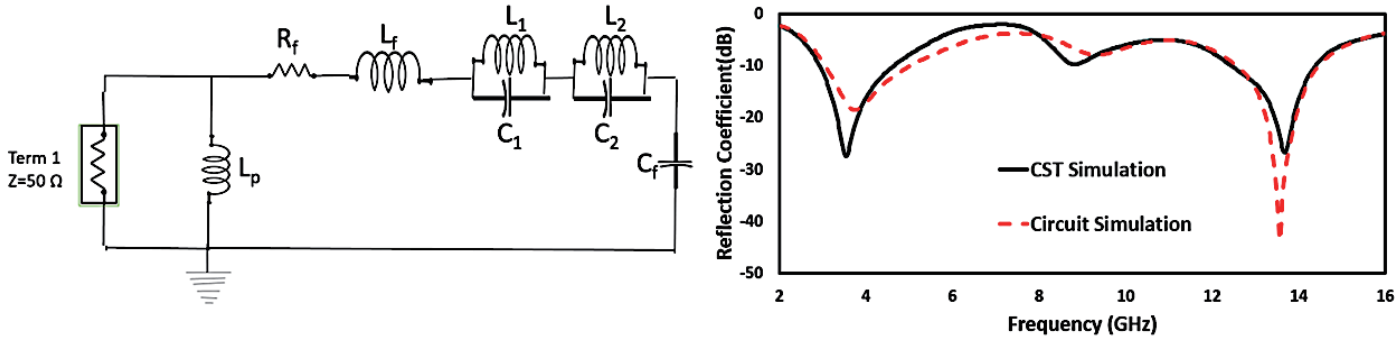

(a) (b)

FIGURE 3. (a) Equivalent circuit model of antenna. (b) Comparison of S_{11}.

TABLE 1. Equivalent circuit parameters and its value

Parameters	Values	Description
L_f	0.88 nH	Feed line series inductance
C_f	0.17 pF	Feed line shunt capacitance
L_p	3 nH	Patch inductance
C_1	1 pF	Capacitance between outer ring trace
L_1	2.059 nH	Inductance of outer ring
C_2	1 pF	Capacitance between inner ring trace and patch
L_2	0.295 nH	Inductance of inner ring
R_f	28.11 Ω	Feed line resistance

The lumped equivalent model using the Keysight ADS makes the antenna performance defensible. The lumped equivalent model of the antenna comprises the patch, ring unit cell, and feed equivalent which are depicted in Figure 3. The transformer-coupled feed is represented by its lumped equivalent series resistance inductance (L_f) and shunt capacitance (C_f). The equivalent of the radiating patch antenna and the inner and outer rings of the unit cell is series inductance (L_P) and a parallel combination of inductance (L_1, L_2) and capacitance (C_1, C_2). The components for the outer ring (L_1, C_1) and inner ring (L_2, C_2) give a lower band (3.5 and 8.5 GHz) response, and the last band corresponds to patch (L_P) resonance. The value of the lumped equivalent parameters is shown in Table 1. The antenna's CST simulation and circuit simulation reflection coefficient S_{11} (dB) are shown in Figure 3(b). It shows that the simulation results from CST Microwave Studio match the circuit simulation. There is a slight difference which may be due to the mutual coupling effect.

4. RESULTS AND DISCUSSION

4.1. Extraction of the Parameter of the Unit Cell

The proposed unit cell size is 10 mm of material FR-4, having a dielectric constant of 4.4 and a loss tangent of 0.0025. The unit cell [20, 21] is a three-layer-type unit cell that gives high gain used in telemetry applications. The bandwidth claimed in papers is nearly 2.5 GHz, while the proposed unit cell gives nearly the same bandwidth in three different bands with a miniaturized response. The proposed unit cell gives the advantage of wide band and high gain property by utilizing the epsilon negative property of metamaterial. To evaluate the behavioral characteristics of the metamaterial unit cell, its effective parameter is extracted, shown in Figure 4. Figures 4(a) and (b) show the retrieval results in permittivity and permeability of the ring unit cells. According to metamaterial theory, if both permittivity and permeability are negative for the operating band, it is known as double-negative (DNG) metamaterial. It is shown in Figures 4(a) & (b) that the real part of permittivity is negative for the initial range of frequency up to 3.5 GHz, and the real part of permeability is switched to the negative region from 3.7 GHz to 6.7 GHz. It confirms that the unit cell exhibits single negative metamaterial (SNG) behavior for resonating frequency 3.5 GHz. This SNG metamaterial suppressed the surface wave efficiently, giving a lower operation band from 2.9 GHz to 4.5 GHz. At the second resonance frequency, the 8.5 GHz unit cell again exhibits SNG characteristics with negative permittivity and positive permeability. However, at 8.5 GHz, the imaginary component of permittivity is high, which results in slightly lossy behaviour at the second operating band. For the resonating frequency of the conventional patch 13.7 GHz, both permittivity and permeability are positive. The imaginary parts of permittivity and permeability are close to zero and one, respectively, ensuring low loss in the operating band.

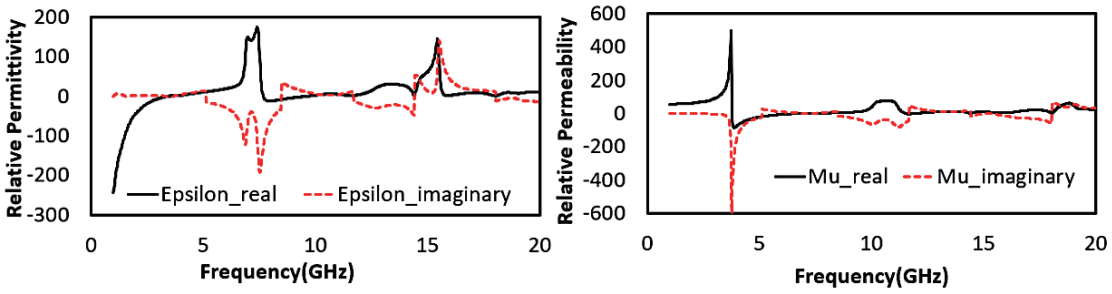

(a) (b)

FIGURE 4. Extracted effective parameters of the unit cell: (a) Real and imaginary effective permittivity (b) Real and imaginary effective permeability.

(a) (b)

FIGURE 5. (a) Experimental set-up of proposed antenna, (a) S_{11}, (b) Gain and Efficiency.

4.2. Reflection Coefficient

The operating principle of the antenna works on the semi-infinite boundary conditions. The semi-infinite boundary of a double positive material (Patch antenna) and an epsilon negative material (Ring metamaterial unit cell) result in two different combinations for the surface wave. These two surface waves propagate such that they couple with each other and exchange energy, which enables wave propagation and gives the desired three-frequency band. Again, metamaterial ring unit cell loading provides a wideband in resonating frequencies due to the capacitive coupling. The proposed antenna is fabricated, and the S-parameter is measured using an Agilent N5230A network analyzer. The experimental setup is shown in Figure 5. There is a small mismatch between the simulated and measured reflection coefficients due to the fabrication limitations. It gives impedance matching below -10 dB in operating bands. The designing steps of an antenna and its corresponding S_{11} parameter are discussed and shown in Figures 6(a) and (b). Firstly, a conventional patch of a given dimension is designed. It gives impedance mismatch throughout the band. Then, impedance matching of the proposed antenna is improved by a quarter-wave transformer-coupled feed line. It provides smooth impedance matching of -18 dB at 11.9 GHz. Next, the metamaterial ring unit cell is loaded in the patch antenna, giving three narrow-band resonance miniaturized responses. The ground at the back of the antenna is then changed to the partial ground, improving impedance matching by widening the band at the operating band. The band was enlarged because of unit cell loading, which increased capacitive coupling and decreased inductive coupling. Thus, the low-quality factor of the antenna is reduced; hence, bandwidth improved parameters. Finally, the proposed antenna's simulated and measured reflection coefficients are given in Figure 6(c). One of the practical applications of the antenna could be as a wearable antenna. A realistic model known as the voxel phantom consists of the complex permittivity and conductivity of the human body tissue and is used to study the wearable application of any antenna. The fabrics used to design wearable antennae operate at the 2.45 and 5 GHz wireless bands. The proposed antenna owns the band 2.9 to 4.5 GHz. However, the analysis of antenna behavior near the voxel phantom is required to confirm the proposed antenna for wearable applications.

4.3. Gain and Efficiency

The simulated peak gain is 1.5, 4.1, and 6.5 dBi in the operating band, as shown in Figure 7. The antenna gain is improved by applying a metamaterial unit cell of the same resonating frequency. In this design, the unit cell has a real and negative value of permeability and permittivity and low imaginary permeability and permittivity, which yields improved gain and low loss. Thus, the loading of the metamaterial unit cell on the proposed antenna gives an additional band at 3.5 GHz with a positive gain of 1.5 dBi without affecting the gain of another band. Moreover, the effective area also increases with the higher frequency, resulting in higher gain at a higher frequency. Thus, gain increases from 1.5 dBi to 3.5 dBi from the lower to upper

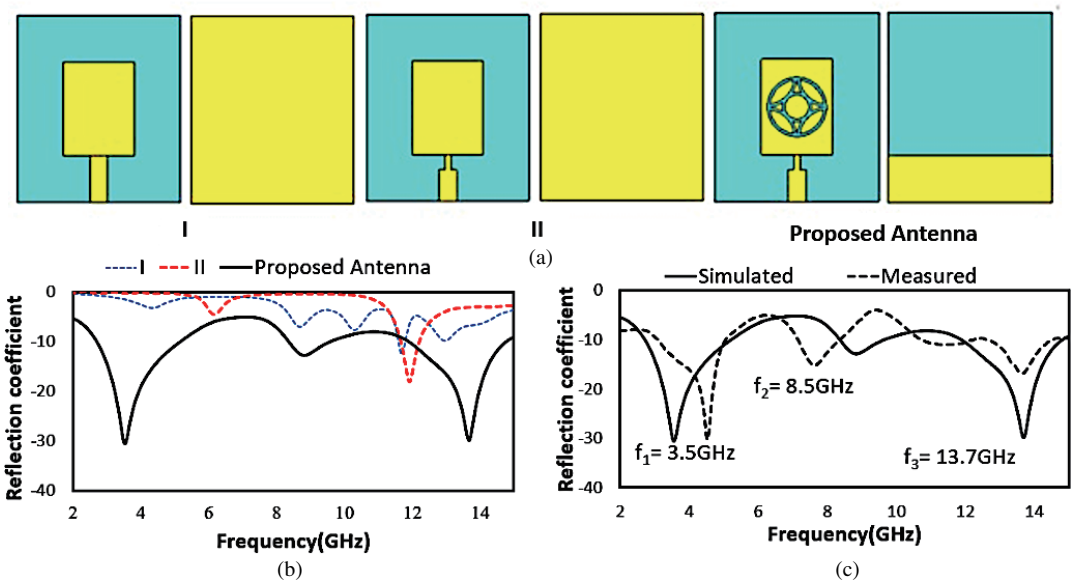

FIGURE 6. (a) Designing steps of the proposed antenna. (b) Reflection coefficient of designing steps. (c) Simulated and measured reflection coefficient.

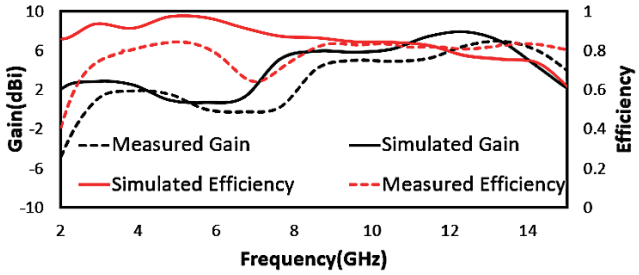

FIGURE 7. Simulated gain and efficiency curve of the proposed antenna.

bands. The antenna radiation efficiency is one of the most important parameters since it is the most useful and informative measure of how efficient an antenna is to radiate or receive the radio wave at a desired frequency. It is defined as the ratio of the total power radiated by the antenna (P_r) to the total power accepted by the antenna (P_a) at its input terminal. The measurement set of efficiency of the antenna comprises a horn antenna used to transmit the signal, and the proposed antenna is used to receive the power in an anechoic chamber. The efficiency is calculated using the formula.

$$\text{Antenna Radiated efficiency} = \frac{P_r}{P_a}$$

The antenna radiation efficiency is subject to the antenna's impedance matching. With the loading of the ring unit cell, better impedance matching is achieved for both operating bands, due to which the efficiency achieved in both bands is more than 75%.

4.4. Radiation Pattern and Current Distribution

An analysis of the radiation behaviour of the proposed antenna at the resonance frequencies 3.5 GHz, 8.5 GHz, and 13.7 GHz is given in Figure 8. Although the measured resonance frequency is shifted slightly to the simulated one, the operating band covers the simulated frequencies, so the radiation pattern is observed at aforesaid frequencies. It is observed that at 3.5 GHz, the antenna behaves as a monopole and radiates omnidirectionally. The radiation patterns at 8.5 and 13.7 GHz are in all directions and give a multilobe pattern with null observed in the negative y-direction.

Figure 9 illustrates the measured and simulated co-polarization and cross-polarization radiation patterns at 3.5 GHz, 8.5 GHz, and 13.7 GHz, respectively. It is observed that the antenna has a nearly omnidirectional radiation pattern at all three resonating frequencies. Moreover, in the E plane, the antenna gives good isolation between co- and cross-polarizations of -20 dB. The antenna gives excellent isolation between co- and cross-polarizations of more than 100 dB in all 360° beam angles in the H plane. Thus, the proposed antenna indicates excellent linear polarization purity. At higher resonating frequencies, the pattern is shifted by an angle of 30° in the H plane, keeping the E plane radiation almost the same. There is a good agreement between the measurement and simulation, and a monopole-like radiation

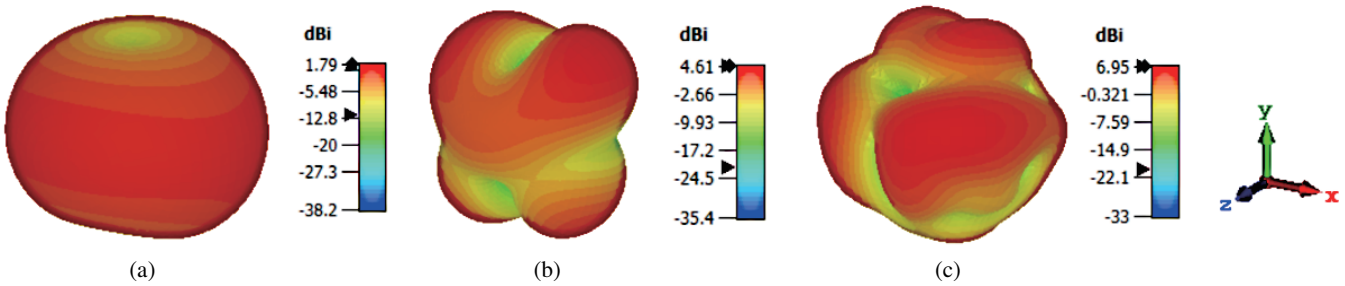

(a) (b) (c)

FIGURE 8. 3D radiation pattern at (a) 3.5, (b) 8.5 GHz, (c) 13.7 GHz.

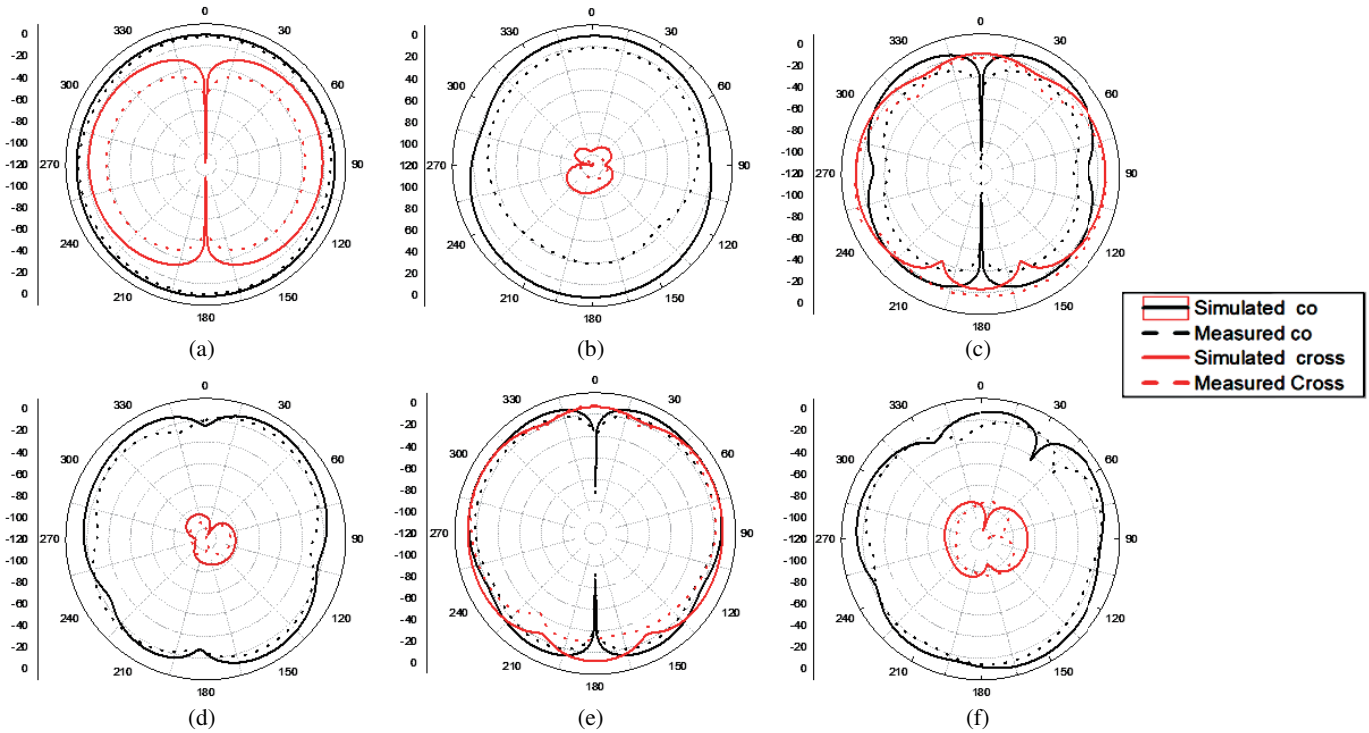

(a) (b) (c) (d) (e) (f)

FIGURE 9. Radiation pattern of the antenna, (a) *E* Plane at 3.5 GHz, (b) *H* Plane at 3.5 GHz, (c) *E* Plane at 8.8 GHz, (d) *H* Plane at 8.5 GHz, (e) *E* Plane at 13.7 GHz, (f) *H* Plane at 13.7 GHz.

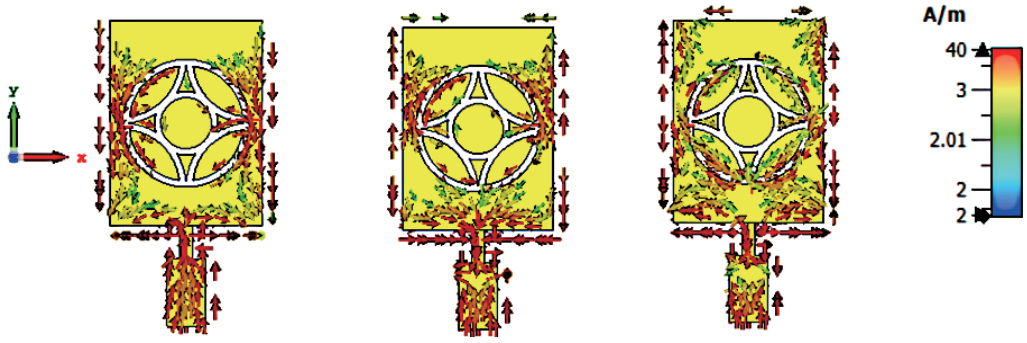

(a) (b) (c)

FIGURE 10. Current distribution at (a) 3.5 GHz (b) 8.5 GHz and (c) 13.7 GHz.

TABLE 2. Comparison of the proposed work with the recently published works.

Ref. No. (Year)	Frequency (GHz)	Electrical size ($(\lambda_o)^3$)	Imp. BW (%)	Gain (dBi)	Efficiency (%
Proposed Antenna	3.5, 8.5, 13.7	$0.32 \times 0.27 \times 0.016$	43, 25, 15	1.5, 4.1, 6.5	< 75
[22] (2019*)	3.1, 5.0, 6.6	$0.48 \times 0.43 \times 0.018$	5.11, 7.33, 11.70	2.72, 3.8, 2.12	41.2, 84.7, 52.8
[23] (2020*)	2.2, 2.8, 3.5	$0.29 \times 0.29 \times 0.018$	4.5, 6, 7	1.5, 6.5, 1.7	NA^*
[24] (2021*)	1.8, 2.4, 5.2	$0.14 \times 0.14 \times 0.01$	2.09, 1.64, 2.71	$-7.25, -1.8, 0.12$	NA^*
[25] (2022)	2.4, 3.2, 6.5	$0.13 \times 0.13 \times 0.12$	4.1, 22	< 2 dBi	60, 78
[26] (2023)	3.02, 4.14, 5.44	$0.97 \times 0.97 \times 0.025$	3, 9, 5	< 4 dBi	NA^*

References with * marks have more than three bands, and only the first three bands have been considered for comparison. NA^* means data not given.

pattern is obtained at each frequency. The current distribution in the radiating element at resonance frequency is shown in Figure 10, respectively. It can be observed that the intensity of the distributed current is more vigorous in the upper band than the lower band. The simulated surface current is concentrated near the antenna's feed line, confirming monopole radiation at 3.5 GHz. Then, as frequency increases, more draft is focused on the top of the patch in the middle band. As a result, the radiation patterns will be gradually close to the y-direction. Moreover, compared to the lower frequency, the current variation at 8.5 and 13.7 GHz is diverse in all directions, resulting in multi-beams. The antenna performance is compared with recently published articles in Table 2. It is confirmed that the proposed antenna gives the widest bandwidth with positive gain and good efficiency.

5. CONCLUSION

A planer miniaturized, quarter-wave transformer-coupled fed multi-band antenna loaded with a metamaterial ring unit cell has been discussed. The frequency bands originated due to the loading of the unit cell and the resonant patch itself. The impedance matching is achieved using a transformer-coupled feed line, which helps to get minimum cross-polarization. The antenna can radiate a good omnidirectional, nearly monopole-like radiation pattern in both bands. The proposed antenna exhibits good radiation performance with positive gain in both bands. It can be easily fabricated to find applications in the 5G sub-band (3.3–4.2 GHz), X band (8–12 GHz), and Ku band (12–14 GHz) for upper resonance.

REFERENCES

[1] Carver, K. and J. Mink, "Microstrip antenna technology," *IEEE Transactions on Antennas and Propagation*, Vol. 29, No. 1, 2–24, 1981.

[2] Liu, Y., L.-M. Si, M. Wei, P. Yan, P. Yang, H. Lu, C. Zheng, Y. Yuan, J. Mou, X. Lv, *et al.*, "Some recent developments of microstrip antenna," *International Journal of Antennas and Propagation*, Vol. 2012, Article ID 428284, 2012.

[3] Quan, X., R. Li, Y. Cui, and M. M. Tentzeris, "Analysis and design of a compact dual-band directional antenna," *IEEE Antennas and Wireless Propagation Letters*, Vol. 11, 547–550, 2012.

[4] Suh, Y.-H. and K. Chang, "Low cost microstrip-fed dual frequency printed dipole antenna for wireless communications," *Electronics Letters*, Vol. 36, No. 14, 1177–1179, 2000.

[5] Liu, Z. D., P. S. Hall, and D. Wake, "Dual-frequency planar inverted-F antenna," *IEEE Transactions on Antennas and Propagation*, Vol. 45, No. 10, 1451–1458, 1997.

[6] Salonen, P., M. Keskilammi, and M. Kivikoski, "Single-feed dual-band planar inverted-F antenna with U-shaped slot," *IEEE Transactions on Antennas and Propagation*, Vol. 48, No. 8, 1262–1264, 2000.

[7] Wong, K.-L., L.-C. Chou, and C.-M. Su, "Dual-band flat-plate antenna with a shorted parasitic element for laptop applications," *IEEE Transactions on Antennas and Propagation*, Vol. 53, No. 1, 539–544, 2005.

[8] Rajeshkumar, V. and S. Raghavan, "Trapezoidal ring quad-band fractal antenna for WLAN/WiMAX applications," *Microwave and Optical Technology Letters*, Vol. 56, No. 11, 2545–2548, 2014.

[9] Beigi, P. and P. Mohammadi, "A novel small triple-band monopole antenna with crinkle fractal-structure," *AEU-International Journal of Electronics and Communications*, Vol. 70, No. 10, 1382–1387, 2016.

[10] Pendry, J. B., A. J. Holden, D. J. Robbins, and W. Stewart, "Magnetism from conductors and enhanced nonlinear phenomena," *IEEE Transactions on Microwave Theory and Techniques*, Vol. 47, No. 11, 2075–2084, 1999.

[11] Shelby, R. A., D. R. Smith, and S. Schultz, "Experimental verification of a negative index of refraction," *Science*, Vol. 292, No. 5514, 77–79, 2001.

[12] Zhu, W., I. D. Rukhlenko, and M. Premaratne, "Light amplification in zero-index metamaterial with gain inserts," *Applied Physics Letters*, Vol. 101, No. 3, 031907, 2012.

[13] Sarkar, D., K. Saurav, and K. V. Srivastava, "Multi-band microstrip-fed slot antenna loaded with split-ring resonator," *Electronics Letters*, Vol. 50, No. 21, 1498–1500, 2014.

[14] Patel, S. K. and Y. Kosta, "Complementary split ring resonator metamaterial to achieve multifrequency operation in microstrip-based radiating structure design," *Journal of Modern Optics*, Vol. 61, No. 3, 249–256, 2014.

[15] Antoniades, M. A. and G. V. Eleftheriades, "Multiband compact printed dipole antennas using NRI-TL metamaterial loading," *IEEE Transactions on Antennas and Propagation*, Vol. 60, No. 12, 5613–5626, 2012.

[16] Balanis, C. A., *Antenna Theory Analysis and Design*, 811, John Wiley & Sons Inc., 2005.

[17] Gautam, A. K., L. Kumar, B. K. Kanaujia, and K. Rambabu, "Design of compact F-shaped slot triple-band antenna for WLAN/WiMAX applications," *IEEE Transactions on Antennas and Propagation*, Vol. 64, No. 3, 1101–1105, 2015.

[18] Kumar, A., M. P. Abegaonkar, and S. K. Koul, "Triple band miniaturized patch antenna loaded with metamaterial unit cell

for defense applications," in *2016 11th International Conference on Industrial and Information Systems (ICIIS)*, 833–837. IEEE, 2016.

[19] Neeshu, K. and A. K. Tiwary, "Metamaterial loaded antenna with improved efficiency and gain for wideband application," *IETE Journal of Research*, Vol. 69, No. 3, 1–8, 2021.

[20] Tuloti, S. H. R., P. Rezaei, and F. T. Hamedani, "High-efficient wideband transmitarray antenna," *IEEE Antennas and Wireless Propagation Letters*, Vol. 17, No. 5, 817–820, 2018.

[21] Nosrati, M., P. Rezaei, M. Danaie, and S. Parvizi, "Wideband transmitarray antenna using electric ring resonator shaped slot element," *Journal of Electromagnetic Waves and Applications*, Vol. 35, No. 15, 2092–2101, 2021.

[22] Saraswat, R. K. and M. Kumar, "A vertex-fed hexa-band frequency reconfigurable antenna for wireless applications," *International Journal of RF and Microwave Computer-Aided Engineering*, Vol. 29, No. 10, e21893, 2019.

[23] Selvi, N. T., P. T. Selvan, S. Babu, and R. Pandeeswari, "Multiband metamaterial-inspired antenna using split ring resonator," *Computers & Electrical Engineering*, Vol. 84, 106613, 2020.

[24] Thankachan, S. and B. Paul, "Metamaterial inspired electrically small multiband monopole antenna using single DNG MTM and ring resonators," 2021.

[25] Milias, C., R. B. Andersen, P. I. Lazaridis, Z. D. Zaharis, B. Muhammad, J. T. Kristensen, A. Mihovska, and D. D. Hermansen, "Miniaturized multiband metamaterial antennas with dual-band isolation enhancement," *IEEE Access*, Vol. 10, 64 952–64 964, 2022.

[26] Jha, P., A. Kumar, and N. Sharma, "A metamaterial inspired split ring resonator accomplished multiband antenna for 5G and other wireless applications," *Revue Roumatine Des Sciences Techniques—Série Électrotechnique et Énergétique*, Vol. 68, No. 2, 127–131, 2023.